

Research Papers

Optimization-based state-of-charge management strategies for supercritical CO₂ Brayton cycle pumped thermal energy storage systems

Alp Albay^{*}, Zhennan Zhu, Mehmet Mercangöz

Centre for Process Systems Engineering, Department of Chemical Engineering, Imperial College London, London, United Kingdom



ARTICLE INFO

Keywords:

Pumped thermal energy storage
Variable speed operation
State-of-charge management
Renewable energy storage
Scheduling optimization
Carnot battery

ABSTRACT

We present a study concerning the state-of-charge (SoC) management strategies for pumped thermal electrical energy storage (PTES) systems. The particular system under study is a recuperative Brayton Cycle PTES with supercritical CO₂ as the working fluid and uses molten salt and water as hot and cold side thermal storage reservoirs. The charging and discharging cycles, including the turbomachinery, heat exchangers, and two-tank thermal storage units are modelled using Aspen HYSYS, considering variable speed operating characteristics of the turbomachines. An in-cycle SoC management strategy is proposed to maintain equal charging and discharging capacities between the hot and cold side thermal storage reservoirs, whereas a cycle-to-cycle SoC management strategy is used to constrain the PTES operating envelope for charge/discharge power and duration given operational objectives. The model is used in several case-studies to demonstrate the SoC management strategies. The case study results showed that, given an electricity price profile, the algorithm can determine feasible charge/discharge profiles while maximizing the operational profit. Additionally, if the PTES system is integrated with a wind farm, it enables the wind farm to provide dispatchable power. The round-trip efficiencies of the system is within the range of 35–60 % and in certain scenarios with increased part-load operation, such as the wind farm integration scenario, the average efficiency is observed to be 46.5 %. The SoC of both tanks displayed a negligible deviation of 0.24 % after five days of operation, including operation under part load conditions. The findings provide a new avenue for revenue stacking via flexible operations and can help accelerate the adoption of PTES systems.

Nomenclature

Symbols

c_p	Specific heat capacity at constant pressure
N	Number of intervals
P	Profit
Q	Heat flow
S	Hot salt tank level
T	Temperature
W	Electrical work
β	Compressor pressure ratio
ϵ	Error for in-cycle SoC minimization
η	Compressor efficiency
η_{RTE}	Round-trip efficiency
λ	Balancing coefficient
ω	Scaling coefficient

Abbreviations

CHP	Combined heat and power
CHX	Cold side heat exchanger
CSP	Concentrated solar power
HHX	Hot side heat exchanger
PTES	Pumped thermal energy storage
Rec	Recuperator
SCBC	Supercritical CO ₂ Brayton cycle
sCO ₂	Supercritical CO ₂
SoC	State-of-charge
TES	Thermal energy storage

Subscripts

c Charging variable

(continued on next page)

^{*} Corresponding author.

E-mail address: alp.albay21@imperial.ac.uk (A. Albay).

(continued)

d	Discharging variable
e	Electrical price
h	Heat price
H	Heating flowrate
s	Molten salt flowrate/surplus power
t	Time interval
w	Water flowrate/wind power

Superscripts

	Discharging variable
--	----------------------

1. Introduction

Total global energy consumption rose from 123 PWh in 2000 to 179 PWh in 2022 [1]. Meanwhile, there is a worldwide imperative to combat climate change, which requires that the generation of power must quickly and significantly shift towards decarbonized energy sources. As essential components of this shift, wind and solar energy carry increased importance [2,3]. Nevertheless, because of their intermittency, raising the proportion of these renewable energy sources to a majority in the generation mix is posing a challenge to the power grid [4], necessitating the development of scalable economical energy storage solutions [5]. Currently, Pumped Hydroelectric Storage (PHS) accounts for 95 % of grid-scale energy storage worldwide [6]. However, there are restrictions for its application, arising from geographical constraints, high capital costs, and water scarcity concerns. One such alternative among the class of thermomechanical energy storage technologies is Pumped Thermal Energy Storage (PTES), which provides advantages over PHS including geographical independence, cheaper capital costs and possibilities for thermal integration with industrial plants and district heating and cooling plants.

A PTES system, also referred to as a “Carnot battery” or electro-thermal energy storage (ETES), stores electrical energy in the form of thermal energy. It works by transferring heat between two thermal reservoirs at different temperatures. Stored energy can be of the form of sensible heat or latent heat, where the heat is stored in the temperature change or phase change of the storage medium respectively [7]. During charging, a PTES system uses excess electricity to drive a heat-pump, simultaneously: (i) providing heat to a hot store, which forms a high-temperature thermal storage reservoir, and (ii) cooling the cold store, i.e., a low-temperature thermal storage reservoir. When electricity is required, the system can be reversed and operated as a heat-engine. PTES systems have the potential to store large amounts of energy (tens to hundreds of MWs) by using scalable and proven power plant components. These systems can operate at large scales without being limited by geography, with roundtrip electrical efficiencies of up to 60 %, long charge and discharge durations (multiple hours), long storage times (multiple days), and lifetimes of up to 30 years (>10,000 cycles). To date, studies of PTES have focused on large-scale applications with different design configurations [8,9] as well as proof-of-concept pilot-plant experiments [10]. However, due to the aforementioned intermittency issues with renewable dominant grids, any storage technology coupled to a renewable heavy grid will need to accommodate variabilities in charging and discharging power demands. Variable power input and output are essential for energy storage systems to operate in order to maximize grid support [11]. This issue creates the necessity for energy systems to operate at off-design (or part-load) conditions. Studies on part-load operation have been limited in previous literature, mainly drawing from part load behavior of power generation cycles [12]. Therefore, it is important to build a comprehensive understanding of the part-load performance of a grid-integrated PTES system.

In its analysis, this paper employs supercritical CO₂ Brayton cycle (SCBC) based PTES systems. Due to low critical pressure (7.3 MPa) and

temperature (31 °C) of CO₂; high efficiency, wide operating range, safety, enhanced heat transfer and low environmental impact can be achieved with SCBCs [13]. These power cycles are proven to be effective in power generation and conversion applications [14,15]. SCBCs have many applications as power generation cycles in nuclear, coal and gas power plants [16–18] as well as more renewable options in concentrated solar power plants (CSP) [19] and waste heat recovery [20]. Having been established in various areas, SCBCs have also gained increased attention in the energy storage field.

Building on the body of research regarding PTES system performance, this study aims to address some of the key gaps identified in the literature. Previous studies on various PTES layouts and technologies applicable to PTES are presented here. The work of Morandin et al. [21] focused on transcritical CO₂ cycles, with latent heat storage on the cold side. Studies by Desrues et al. [9] and Ma et al. [22] demonstrated that PTES systems using packed bed solid storage media are competitive with technologies like PHS and CAES. Furthermore, the integration of PTES and SCBC systems with concentrated solar power (CSP) plants has been extensively explored in works such as [23–25]. Frate et al. [26] contributed by analyzing the off-design performance of a closed Brayton PTES system with packed bed storage, while Yang et al. [27] investigated PTES layouts under part-load conditions specifically for power generation. Lastly, Xingyan et al. [12] focused on the efficiency improvements from reheating and intercooling recompression cycles in sCO₂ Brayton cycles, despite the increased cost and complexity.

Recently, as part of the Arpa-E DAYS program, Echogen operated a pilot scale 100 kWth supercritical-CO₂ thermal cycle using solid hot storage and phase change materials on the cold side. The cycle wasn't fully developed but it demonstrated principals of operation and control of process components [28] Elsewhere, researchers at the Southwest Research Institute developed a 5 kWe pilot facility, utilizing an air cycle [29]. They investigated the efficacy of different control methods such as inventory control, working fluid recycle and turbomachinery speed control. It was found that the main challenge stemmed from controlling the ramp-up phase of the transient behavior, exacerbated by the inefficiencies due to heat loss in the system. McTigue and Neises focused on off-design operation with inventory control [30]. The process they studied is similar to the one studied in this paper, as both employ a variation of the Brayton cycle with liquid storage and CO₂ as the working fluid. However, the main tool of part-load control is inventory control, whereas in this study, the part-load operation is satisfied by turbomachinery speed control.

This study makes its design choices by building on these previous studies. Since there are no to-scale, fully operational PTES systems, these decisions come from either component specific designs such as those by Echogen or from other fields such as CSP plants [23] or general power cycles [12,27]. So, while there may be still be insight gained from optimizing PTES design, this is not within the scope of this study.

While these studies have significantly advanced our understanding of PTES systems, one area that remains underexplored is the development of a reliable metric to predict and manage the state-of-charge (SoC) for these systems. Unlike electrochemical batteries, where SoC is a well-established concept, PTES systems require a more nuanced approach to SoC management due to the complex interplay of storage media availability and temperature within the thermal storage tanks. Accurately estimating and managing SoC both within a single cycle and across multiple charging and discharging cycles is crucial for optimizing PTES performance. Therefore, this study seeks to fill this gap by proposing a novel approach to SoC estimation and management for PTES systems, which has been a central focus of our research.

The aim of this study is to understand the part-load behavior of a supercritical CO₂ Brayton cycle PTES system. Rigorous analyses of part-load operation and state-of-charge (SoC) management have seen limited prior research. Consequently, this paper presents a unique contribution to the field of PTES technology. Very recently, Pettinari et al. [31] studied the part-load operation of a heat pump system using a detailed

model. However, that study lacks the scope of a complete PTES system as it does not analyze the heat engine part, which is vital for understanding the part-load behavior of the storage system holistically. Similarly, Ghilardi et al., [32] presented a holistic approach to managing SoC in a cogeneration setting with multiple heat and electricity users. However, this analysis is based on very high-level models without much detail in part-load operation. The contribution of our work is a detailed analysis of both the charging and discharging sides of the PTES process, including a rigorous compressor model and the detailed treatment of the heat exchanger profiles, which was lacking in previous literature. Furthermore, a SoC management strategy in part-load operation for in-cycle and cycle-to-cycle management of the storage inventories is developed. The performance of the proposed approach is demonstrated in several case studies involving a realistic scenario taken from recent historical operation of the United Kingdom national power grid as well as a wind farm integration scenario.

2. System description

The modelling work was conducted in Aspen HYSYS [33]. The charging and discharging cycles were modelled as separate processes, connected by the storage temperatures. The equipment for the processes includes a compressor, an expander, a turbine, two storage heat exchangers and recuperator heat exchanger. The layout of the PTES system is shown in Fig. 1: (a) Charge process; (b) discharge process.

This work is based on the patented recuperative thermoelectric energy storage process by Morandin et al. [21]. A recuperative Brayton cycle exchanges heat internally, reducing wasted heat. This method also offers higher thermal efficiency by increasing the temperature difference between the two sides. It also boasts a relatively simple structure [12]. The storage media are both liquid at the operating temperatures and atmospheric pressures. This reduces the risks associated with using high-pressure containment at non-atmospheric conditions. The hot storage medium is a molten salt mixture called Solar Salt (40 % NaNO_3 and 60 % KNO_3) [34] with a wide operating range, between its melting point of 220°C and a degradation point of $\sim 600^\circ\text{C}$ [35]. It has been widely used in the CSP field. Water was chosen as the cold storage medium due to its high heat capacity, safety and abundance.

Fig. 1 illustrates the layout of the process. During the charging phase (Fig. 1a), CO_2 is compressed to a high temperature and pressure (6 to 1). This high-temperature, high-pressure CO_2 then transfers heat to the molten salt, heating it from 420°C to 560°C under nominal conditions. Next, the CO_2 exchanges heat with low-pressure CO_2 in the recuperator, cooling it down (2 to 3). The cooled CO_2 is then expanded through the expander (3 to 4, Exp). After expansion, the CO_2 is further cooled by a cooler to a temperature slightly above the critical temperature (4 to 4a).

The cooler here helps increase system efficiency and consistency by keeping the cold heat exchanger (CHX) inlet low and constant. Following the cooler, the CO_2 enters a cold heat exchanger (CHX), where it is reheated (4a to 5) while cooling water (9 to 10). CO_2 is preheated in the recuperator (5 to 6) before completing the cycle.

During the discharge process (Fig. 1b), hot molten salt flows through the hot heat exchanger (HHX) increasing the temperature of CO_2 (2' to 1'). The CO_2 then enters the turbine where it is expanded and generates electricity. After the temperature and pressure drop (1' to 6'), the CO_2 is further cooled (6' to 5') in the recuperator and enters the CHX, where it heats water (10' to 9') while cooling itself (5' to 4a'). The CO_2 is then cooled even further by the cooler (4a' to 4') before entering the compressor, which raises its temperature and pressure (4' to 3'). Finally, before beginning the next cycle, the CO_2 passes through the recuperator and is reheated by hot CO_2 (3' to 2').

One process component that stands out from the similar recuperative PTES systems is the addition of a cooler in both cycles instead of one. In every PTES system, some form of heat rejection is required to manage heat accumulation in the system. In this study, one cooler in each cycle was used to distribute this heat rejection. The coolers were placed in the cold side of the process to benefit from cooling close to ambient temperatures. On the discharge side, the cooler ensures that the inlet conditions of the compressor remain constant. Between the CHX and the compressor, the working fluid is close to its critical point. Due to this, any deviation in temperature and pressure induces extreme variations in the properties of the fluid which causes the compressor to behave sub-optimally [36]. The cooler on the charge cycle is less vital than its counterpart in the discharge cycle, but it serves a simple purpose: keeping the cold-water temperature constant throughout different loads, simplifying the process model. Thus, it is bypassed in an ideal design point operation. This is evident when comparing the two T-s diagrams in Fig. 2. The cooler simplifies the process for part-load operation while ensuring there is a large temperature difference between the hot and cold sides, amplifying efficiency. The T-S diagrams show in Fig. 2 are for: (a) Charge process; (b) Discharge process.

The design of the current system operates with a pressure ratio of 2.69 at the design point, which results in a high-pressure side of 19.95 MPa and a compressor outlet temperature of 564.2°C for the charging cycle. These pressures are comfortably in the operating ranges for certain kinds of Printed Circuit Heat Exchangers that are usually utilized in systems such as this [37,38]. Table 1 lists the design point parameters. Bold parameters are those that were determined in the initial conceptual design phase and the others are calculated by the model. The round-trip efficiency, considering the charging and discharging durations, was 59.8 %, which is in the range for comparable thermo-mechanical energy storage technologies.

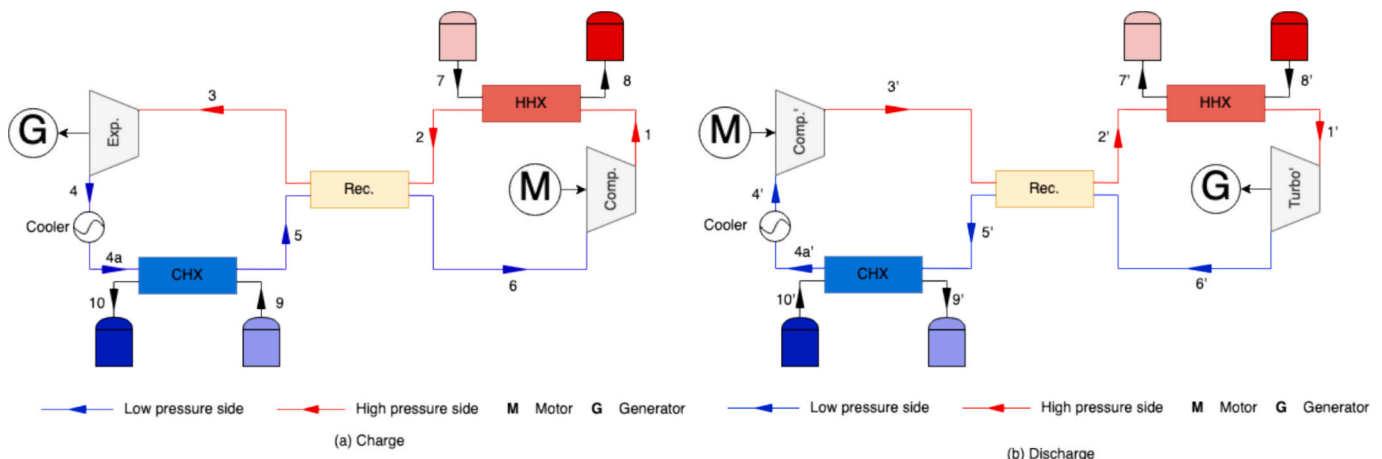


Fig. 1. Layout of the modelled PTES system.

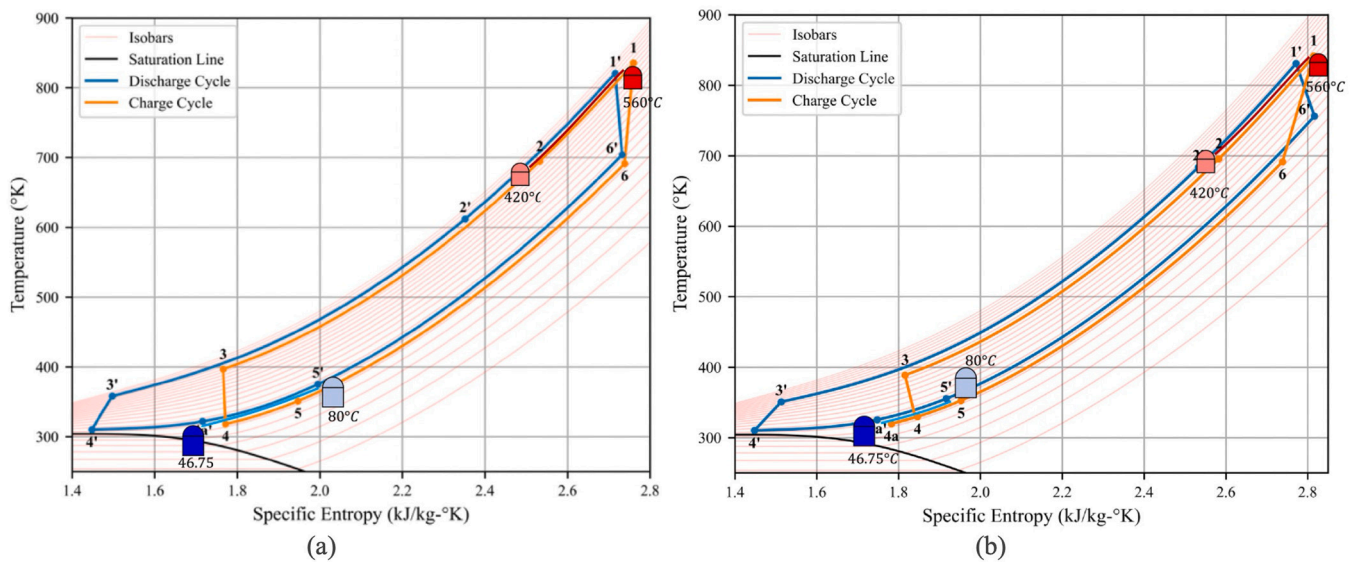


Fig. 2. T-s diagram of the process at design point (a) and a part-load condition (b). Tanks represent the storage material and shows storage temperature. CO₂ property data obtained from REFPROP [39].

Table 1
Cycle properties at design conditions.

Parameter	Charging	Discharging
Compressor work (MW)	8.43	1.51
Turbine/expander work (MW)	2.04	6.86
Net work (MW)	6.39	5.35
Cycle pressure (MPa)	7.40/19.95	8.45/22.17
Compressor efficiency	0.90	0.90
Pressure ratio	2.69	2.62
CO ₂ flowrate (t/h)	19	19
Molten salt flowrate (t/h)	186.4	261.4
Water flowrate (t/h)	72.0	101.0
Duration (h)	8	5.71
Molten salt temperature (°C)	563.2/420	
Water temperature (°C)	80/46.75	
Molten salt tank size (kt)	1.491	
Water tank size (kt)	0.576	

Some assumptions are made for modelling:

- 1) The pressure drop in pipes and heat exchangers are negligible;
- 2) Mass flow rate is constant across the cycle;
- 3) No heat loss from the storage tanks to the ambient.

In this study, the system-wide charging and discharging models were developed using established sub-block models available in ASPEN HYSYS and these sub-blocks can be considered validated. The primary challenge, and the contribution of this paper, lies in parameterizing these models with appropriate performance data. In this work, we derived parameters and performance metrics (e.g., compressor maps) from published references and equipment manufacturer data. The key components that affect performance, especially under part-load conditions, are the turbomachinery. Although full-scale PTES systems have not yet been extensively deployed, many comparable systems exist and serve as a solid foundation for conceptual and exploratory studies.

3. System modelling

The goal of this study is to build a PTES model that can be used to analyze part-load behavior and implement state-of-charge management techniques. Firstly, compressor models are required to implement part-load capabilities to the model as the compressor dictates the load

condition of the system. How these models are built are explained in Section 3.1. Next, in Section 3.2, a detailed explanation of how the internal SoC is managed is presented. The operating envelopes of the compressors and temperature cross considerations are satisfied in this step, ensuring consistent and reliable operation. This model was simulated at different load conditions to generate data for further case studies. This data and the results of the part-load studies are presented in Section 3.3.

3.1. Compressor performance maps

When working at part-load conditions, the most crucial PTES process unit to model is the compressor. Compressor maps are proprietary information of manufacturers. It is thereby challenging to find compressor data that is appropriate for a specific design case. This work adapts a map generation method developed by Tsoutsanis et al. [40] to fit the requirements of the PTES process. The method models speed lines in the pressure ratio vs. mass flow and efficiency vs. mass flow spaces by fitting each line as an ellipse. The intercept points of the ellipses were parameterized with respect to the compressor speed. The surge line was modelled as a line using a cut-off value on the pressure ratio axis as the slope. To adapt the maps to the current process, the equations were analytically solved to produce equations for each parameter. This provided 6 degrees of freedom, which was used to designate the efficiencies and the speeds of the design point and two part-load conditions. The generated compressor map is shown in Fig. 3. Since, the focus of the study was on compressor design, turbine maps were not considered for simplicity. It was assumed that the part-load behavior of the turbine efficiency followed the efficiency of the corresponding compressor in the charging or discharging cycles.

3.2. In-cycle SoC management algorithm

Fig. 4 shows a flowchart of the PTES system modelling and in-cycle state-of-charge management which is needed to account for charging and discharging times by adjusting storage flowrates accordingly. In-cycle SoC management is required for the steady-state part-load modelling of the PTES system. Variables determined in the design phase form the backbone of the HYSYS model and these remain unchanged for all conditions. These variables are: the lower pressure (P_L), compressor inlet (T_6), cold salt tank (T_7), both water tank temperatures (T_9, T_{10}) and

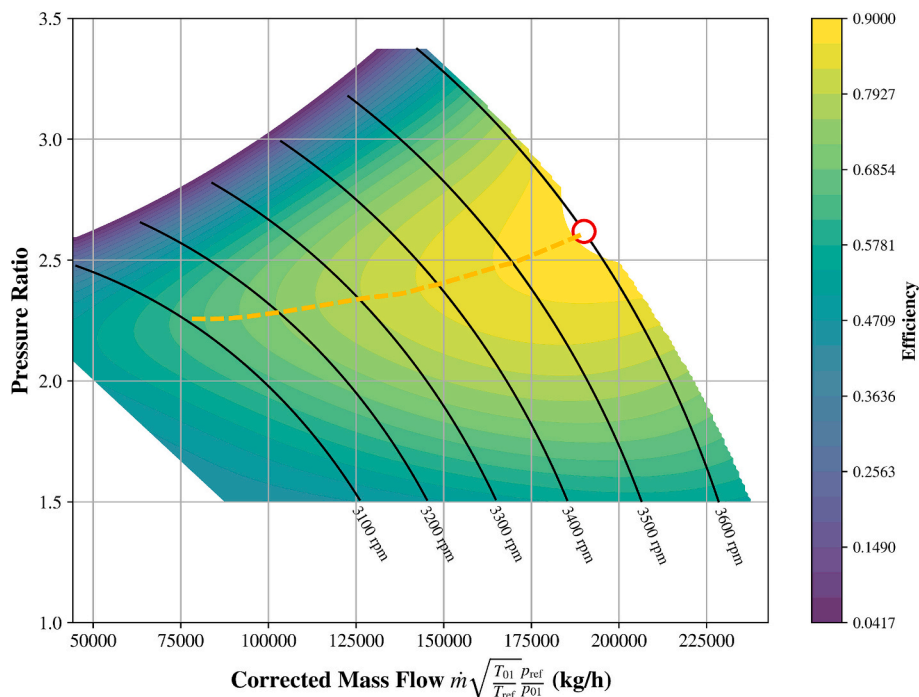


Fig. 3. The generated compressor map. Dashed line represents the operating curve.

their complements in the discharging cycle (denoted with an $'$ in the figures) as well as the discharging cycle compressor inlet temperature (T_4') (Fig. 4a). Setting the compressor speed n , CO_2 flowrate \dot{m}_{CO_2} and a minimum allowed approach temperature ΔT determines the load condition (Fig. 4b) which, in turn, outputs efficiency, η , and a pressure ratio, β (Fig. 4c). With all requisite variables determined, the rest of the model can be solved, albeit without enforcing SoC equilibrium in the tanks.

An optimization algorithm is adopted to equilibrate the operating times of the hot and cold tanks in each cycle individually to make both sides operate for the same duration in each cycle which enforces in-cycle SoC equilibrium. Ideally, this would involve changing the flowrates of the storage fluids to control how fast the system charges and discharges. However, due to limitations imposed by the modelling software, the optimization problem cannot effectively control the flowrates. Instead, the CO_2 temperatures around the two heat exchangers (T_2, T_5, T_2', T_4a') are controlled, to indirectly change the flowrates of the storage fluids. The solver tries to minimize both the mismatch between the operating times of the storage media (ε_i) and the approach temperatures ($\Delta T_{\text{pinch},j}$). The objective function is a normalized (ω_1, ω_2) sum of these two performance indicators.

Charging and discharging durations depend on the sizes of the storage tanks. However, since the Aspen model is only a steady-state model, the storage tanks were not modelled. Their sizes were determined by the design point. The system is designed to charge for 8 h at nominal operation (t_{dp}). So, for the case of the design point, the optimization problem has an additional constraint of the hot and cold charging times ($t_{\text{h}}, t_{\text{c}}$) being 8 h. The resulting flowrates are multiplied by 8 h which outputs the tank sizes. In subsequent simulations (for the other load conditions) these sizes are used to calculate the operating times.

3.3. Part-load performance

Each part-load condition was modelled using the method outlined in Section 3.2 Fig. 5a shows the round-trip efficiency change over the 6 different load levels. Efficiencies were calculated from charge and discharge conditions at matched load levels. Fig. 5b demonstrates that the major decrease in efficiency arises during discharging. Discharge

load falls off much more rapidly than charge load and even though the durations equalize towards the lowest loads, this isn't enough to compensate for the loss in discharging efficiency. Turbomachinery efficiencies dominate the change in overall cycle efficiency in these systems. Although during map generation, both charge and discharge compressor maps were designed to be identical, the method used had limitations and couldn't replicate the charging compressor exactly for discharge. This may be one of the reasons behind the sharp fall in discharge load.

At each part-load condition, temperature of the charging compressor outlet varies. This leads to changing hot salt storage temperature. On the cold storage side, this was mitigated with the introduction of a cooler to keep the HX1 CO_2 inlet temperature constant. The changing temperature profile over decreasing load levels is shown in Fig. 5c. Initially, as load decreases the outlet temperature also decreases. However, at very low loads, temperature sharply increases. This is due to the nonlinear relationship between pressure ratio, efficiency, and inlet temperature.

Since the hot salt temperature varies with each part-load condition, the storage temperature inside the hot salt tank may not be uniform. For the purposes of this study, it was assumed that the molten salt storage temperature would be uniformly mixed, i.e., there would be no temperature stratification forming. However, it is also important to study this stratification phenomenon in future studies.

An important research gap identified by the authors was the lack of understanding of detailed heat exchanger performances in PTES systems. This will allow achieving a better understanding of the heat exchanger requirements of a PTES system when operated at part-load conditions. The heat exchanger sizes are determined by two aspects of the processes: overall flowrates going through the heat exchanger and the pinch point. As the conditions of the process change, so does the pinch point. Consequently, as the results also show, both specifications affect heat exchanger sizes, although there are regimes where one is dominant over the other.

As sCO_2 gets closer to its critical point, the C_p of the fluid becomes more sensitive to changes in temperature. This leads to nonlinear profiles in the temperature vs heat flow plots. Shown in Fig. 6, as the part-load condition varies, so does the temperature profile of the working fluid which changes the place at which the pinch point is observed. The

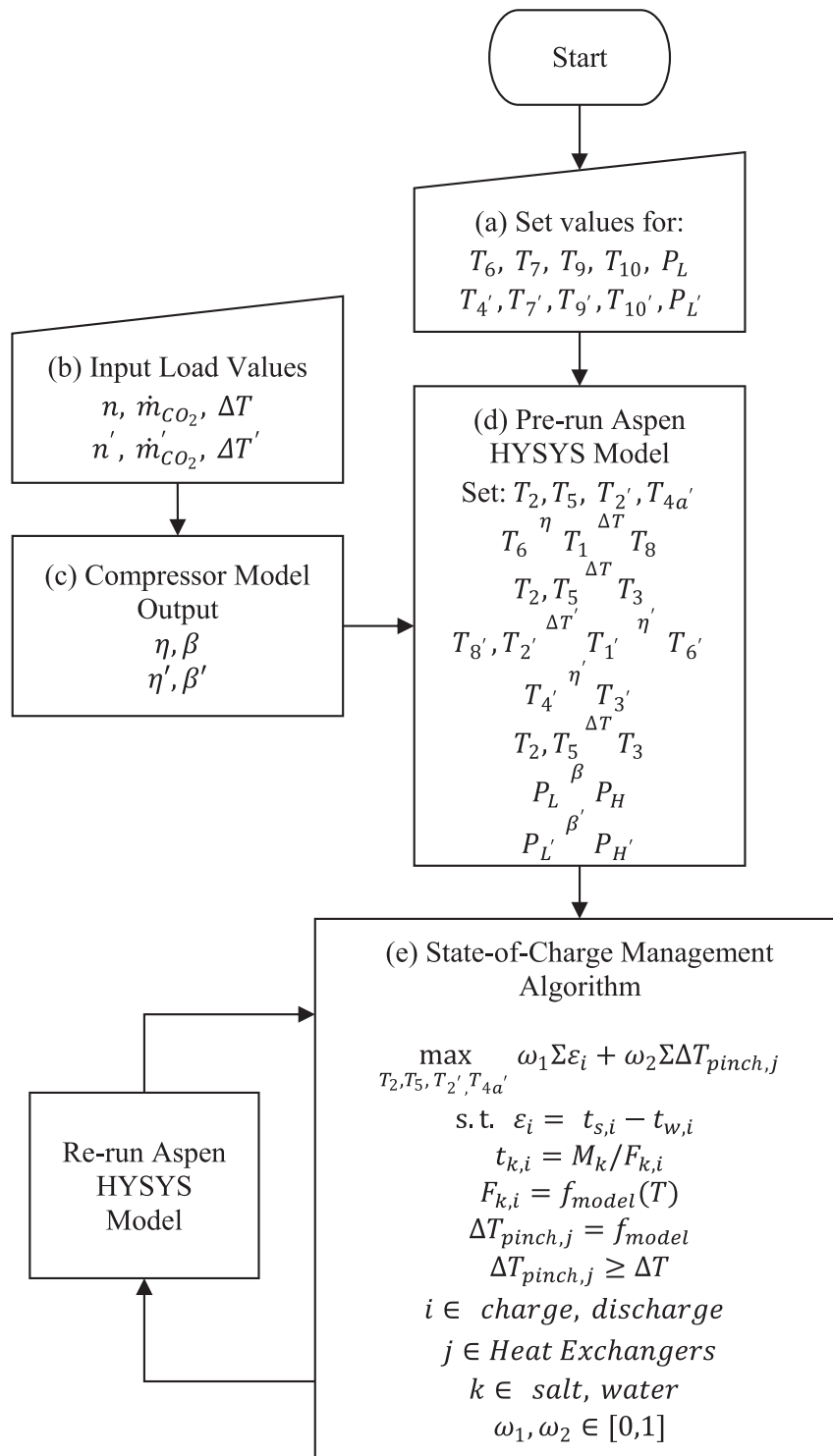


Fig. 4. Flowchart of PTES system modelling and in-cycle state-of-charge management.

pinch is also controlled by the optimization problem, which operates to keep the pinch above and close to 0.5 °C. So, in addition to the position of the pinch point, the size of the pinch changes with each part-load condition. For example, as Fig. 6 shows, in the discharge cold heat exchanger, the smallest pinch point is in the 64.42 % load condition around the 0.3 mark on the heat flow axis. The most interesting interactions appear in the cold side heat exchanger. On the host side, throughout the load levels, the material properties of the CO₂ are relatively constant. Only the size requirement changes with the load. This

fact highlights the need for modular heat exchangers to be used in variable operation of PTES systems. A more rigorous analysis is required to investigate the heat exchanger geometries.

4. System operation

After the model was built in Aspen, the part-load results were used to simulate operation of the PTES system in various conditions. The cycle-to-cycle SoC management is presented in this section since it is

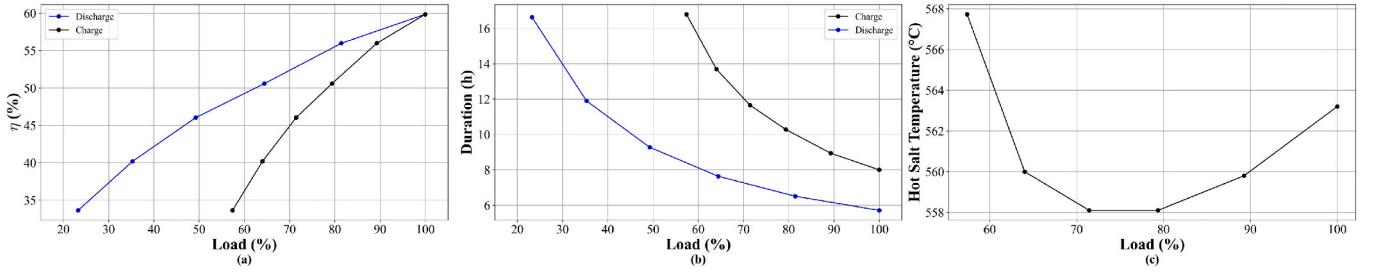


Fig. 5. a) Cycle efficiency vs load curve for each both cycles. 100 % load for each cycle is the design point power and all other load values are calculated relative to this. b) Cycle maximum duration variation at each load condition. c) Charging cycle compressor outlet change at load condition.

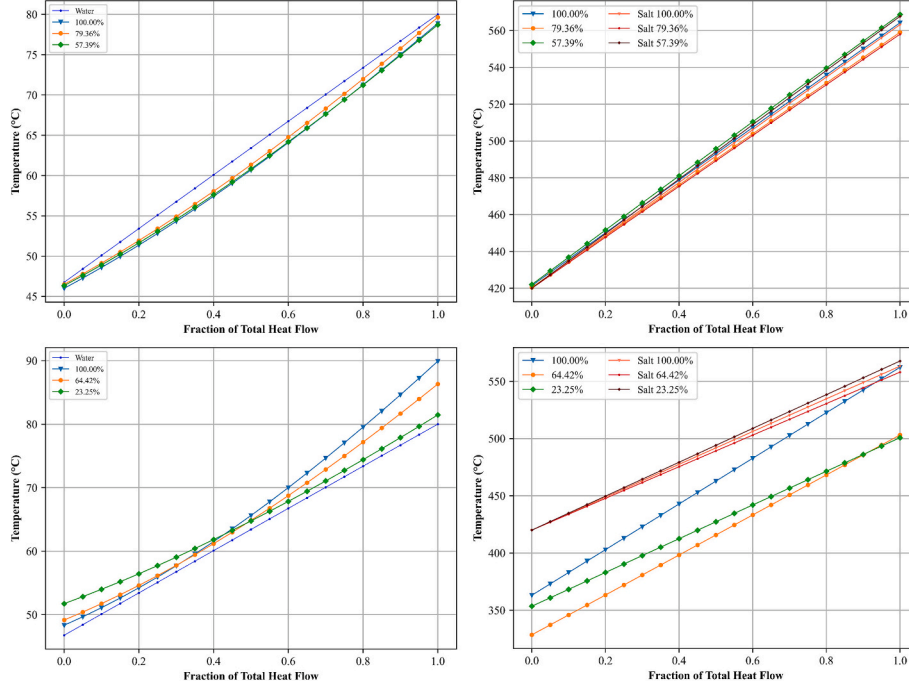


Fig. 6. Internal temperature profiles of heat exchangers for selected operating loads. Left side: CHX, Right side: HHX, with the top row showing charging cycles and the bottom row shows discharging cycles. For all operating loads, see Appendix A for enlarged figures.

inextricably linked with overall system operation. First, a method for estimating and managing cycle-to-cycle SoC is presented in Section 4.1 in the form of an optimization problem. This problem is used in the following sections to simulate several case studies to demonstrate the performance of the PTES system as well as the SoC management methods.

4.1. Cycle-to-cycle SoC management

As opposed to in-cycle SoC management, cycle-to-cycle management involves scheduling and thus cannot be studied in Aspen HYSYS. Instead, the Aspen model was used to generate data at different operating points. The algorithm outlined in Section 3.2 was simulated for 6 charging and 6 discharging points which gives 36 charge/discharge combinations. This data was used to fit storage flowrate vs. system power curves, which allowed for capturing the part-load dynamics without complex simulations each time. These curves were then used to run an optimization problem, shown in Eqs. (1)–(9), minimizing operating cost, given a price profile over at time horizon. For this, the UK grid was used to provide a sample price profile. Data from the Nord Pool Day-Ahead Market was used to generate an average 5-day price profile [41] shown in Fig. 7. The hourly data was aggregated into 5-day horizons.

$$\max_{W_{d,t}, W_{c,t}} \sum_{t=1}^T E_t (W_{d,t} - W_{c,t}) \quad (1)$$

$$\dot{m}_{s,t} = \sum_{n=0}^3 (f_{c,n} W_{c,t}^n - f_{d,n} W_{d,t}^n) \quad (2)$$

$$S_1 = S_0 + \dot{m}_{s,1} \quad (3)$$

$$S_t = S_{t-1} + \dot{m}_{s,t}, t > 1 \quad (4)$$

$$W_c * W_d = 0, \forall t \quad (5)$$

$$W_c \in [0, W_{c,max}] \quad (6)$$

$$W_d \in [0, W_{d,max}] \quad (7)$$

$$S \in [0, S_{max}] \quad (8)$$

$$t \in \{1, 2, \dots, T\} \quad (9)$$

f_c and f_d are the polynomial coefficients of the fits, essentially representing the PTES model. The state-of-charge of the hot side is tracked

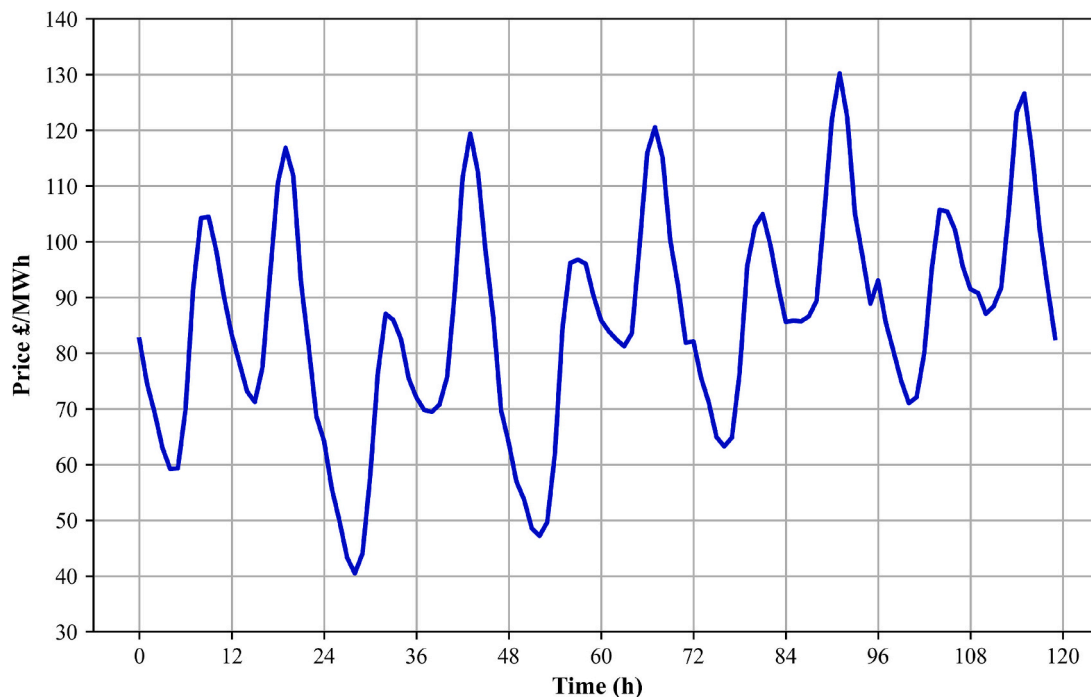


Fig. 7. Average electricity price profile over 5-days in 2023. Based on the UK grid. [41]

by S_t , where it is a function of the salt flowrate $\dot{m}_{s,t}$ and the previous SoC level S_{t-1} . The system is forced into either charging or discharging mode by Eq. (5), by ensuring that at least one is 0.

4.2. Energy trading case studies

As this paper has introduced early on, there were two distinct aspects of SoC management: in-cycle and cross-cycle state-of-charge management. To demonstrate both the capability and the application of both

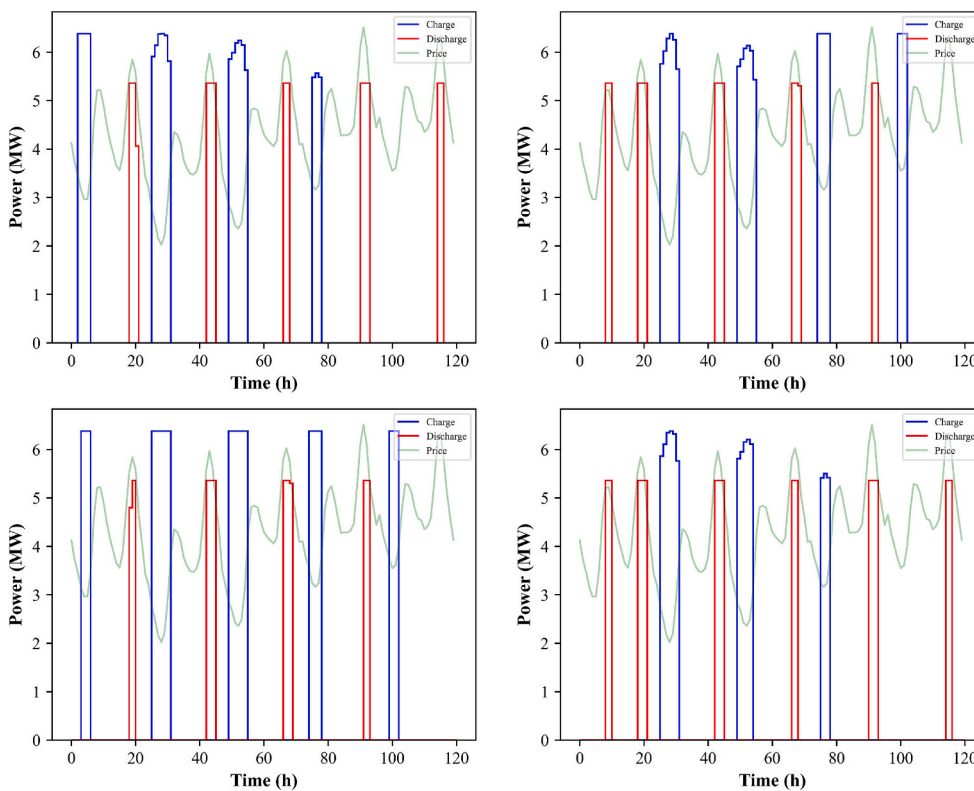


Fig. 8. Optimal charging and discharging profile for case studies (clockwise from top left) 1, 2, 3 and 4. The green line represents the price profile used in the simulation (Fig. 5). It is included here not for quantitative purposes but for qualitative analysis for the reader. (For interpretation of the references to color in this figure legend, the reader is referred to the web version of this article.)

types of SoC management, this work includes several case studies. Previously, Yang et al. [27] conducted a power profile analysis of a SCBC process used for power generation applications. Presented here, is a similar study conducted using the PTES model, considering both charging and discharging operation. The model was represented in the optimization problem by fitting curves to the flowrate vs. power. This model was used to generate a charge/discharge profile, maximizing the profit of the process over a given time horizon and price profile (Fig. 7). The charging and discharging power were discretized into hourly segments. Power of each segment was used to get corresponding flowrates, which in turn was used to calculate SoC at each time interval.

It is impossible to analyze cycle-to-cycle and in-cycle SoC management independently. Although they are implemented at different steps of the modelling process, they are inherently interlinked, and both require the system to be simulated over a given time-horizon. So, there were four case studies conducted, differentiated by their initial conditions and end constraints.

1. Empty start: 0 % tank SoC initial condition, no end-constraint.
2. Full start/Full end: 100 % tank SoC initial condition, >98.5 % tank SoC end constraint
3. Full start: 100 % tank SoC initial condition, no end-constraint
4. Empty start/Full end: 0 % tank SoC initial condition, >98.5 % tank SoC end constraint.

The resulting operating profiles of each case study are shown in Fig. 8 in clockwise order from top left. Charging and discharging power values were mostly around nominal values. These values provided the highest efficiency for the system. Additionally, as Fig. 8 shows, the system allocated charging and discharging to appropriate times according to the price profile. Charging when price is low and discharging when prices are high. One additional observation is that, when there was no end constraint imposed, the optimization problem always gave a solution with 0 % charge level at the end as it is not profitable to have charge left over in the tank at the end of the simulation.

The optimization problem was solved using Pyomo suite in Python with the SCIP [42] and IPOPT [43] solvers operating sequentially. SCIP was used to obtain a solution to provide a warm start for IPOPT.

At these power loads, temperature of the compressor outlet barely changes and consequently the storage temperature barely changes as well. This affirms the assumption made about uniform storage temperature in Section 3.3. Since the change in storage temperature is minimal,

it is safe to assume that temperature, at least for the system simulation at hand, doesn't play a major role. This assumption simplifies the optimization formulation significantly since the compressor outlet temperature vs. power has a very nonlinear profile (Fig. 5). This assumption eliminates the possibility of investigating effects of temperature stratification, but this was deemed outside the scope of the study.

Fig. 9 shows the SoC profiles of each simulation. During each case study, the tank limits were never breached, and the tank capacities were tracked accurately. Although it is hard to see, there are two storage profiles, one for each storage medium. This close match between the salt and water storage capacities affirms the effectiveness of the performance of in-cycle SoC management.

4.3. Wind farm integration study

While the initial case studies demonstrate that the SoC management algorithm works, they don't show the full capabilities of the PTES system. To demonstrate the applicability of a PTES system operated with an SoC management algorithm, there needs to be a more realistic analysis. For this purpose, an additional study is conducted in which the PTES system is coupled with a wind farm. The goal of this study is to demonstrate that the PTES system can aid in the profitability and dispatchability of the wind farm. There are only a few changes needed to adapt the simulation to this scenario.

$$\max_{W_{d,t}, W_{c,t}} \sum_{t=1}^T E_t (W_{d,t} + W_{s,t}) \quad (10)$$

$$W_{w,t} \geq W_{c,t} \quad (11)$$

$$W_{s,t} = W_{w,t} - W_{c,t} \quad (12)$$

Eq. (10) replaces the objective function (Eq. (1)) and Eqs. (11) and (12) are added to the optimization problem. In this scenario, the PTES system would be charged from the coupled wind farm instead of the grid, so a wind supply profile is needed. This profile is obtained from Gridwatch UK [44] for 2023. Both the price profile in Fig. 5 and the wind supply profile are from the UK and from 2023 so that there is a correlation between them. Similar to the electricity profile, the yearly wind profile is averaged over 5 days in hourly intervals. The wind power profile is also scaled to be compatible with the capacity of the PTES model. Charging power at time t , $W_{c,t}$, is capped at the wind supply, W_w ,

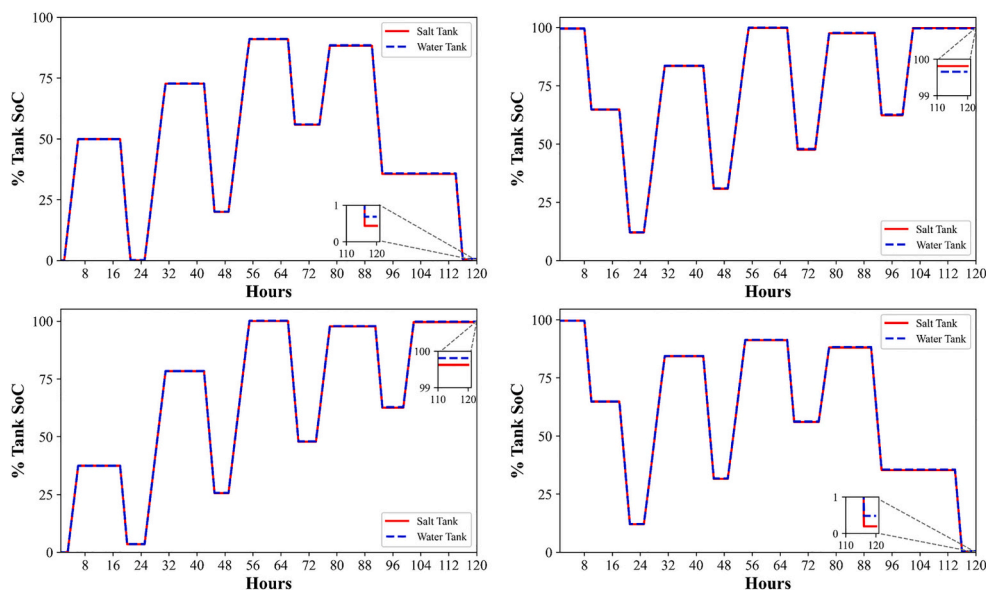


Fig. 9. Comparison of SoC levels between the two tanks. The last 10 h is highlighted in the insert. Case studies 1, 2, 3 and 4, clockwise from top left.

Since the purpose of this case study was to demonstrate the capability of cross-cycle SoC management, the simulation is not finely tuned. For example, at the beginning and end of each charging or discharging interval, the power increases sharply to the desired level. In reality, this may not be feasible, as there should be ramp-up and ramp-down rate considerations. This weakness can be remedied by adding additional constraints. For instance, if the system is used for frequency response or grid support roles, it may be required to operate at unreasonable times (during an emergency when the system frequency falls below a certain level), but those operations add additional value other than monetary value to the system. For these instances, addition of a lower baseload SoC limit can be beneficial. This optimization problem and case study forms the basis of such avenues of research.

Additionally, the system was limited by the charging rate, i.e., the maximum charging or discharging powers. With the given price profile, the lucrative operation ranges were very narrow and this, coupled with the maximum operating powers of the system, limited how much the system can charge and discharge in the simulation. For instance, consider Case 1. There is a low-price region around hour 100. It might make sense to charge in this region but given that there is a limit to the discharging power, and the next discharging window (around hour 115) is narrow, there wouldn't be enough time to discharge the excess charge from hour 100. This leads to reduced operating times, but this is the optimal result.

5.3. Wind farm integration results

Fig. 10 shows the results of this study. On the left-hand side, it is shown that the added constraint of charging with wind power forces the PTES system to operate at lower power during charging, which affects the overall efficiency of the system. Consequently, the round-trip efficiency of this simulation is only 46.5 %, a marked decrease from the initial case studies. This, again, highlights the need for the analysis of part-load operation when working with variable renewable energy sources.

More crucially, the PTES-wind farm coupling allows for time-shifted operation, and as a result, an increase in profit, of the wind farm. On the right-hand side of Fig. 10, the dashed line represents the electricity sold whereas the solid line represents the baseline wind profile. Most of the time, these two lines are the same as the wind farm is outputting wind power directly. However, with the addition of the PTES system, when electricity price is low, instead of immediate dispatch, wind power is stored. This stored power is then dispatched when electricity price is higher in addition to the given wind output. This is evident in the deviations between the profiles. These deviations also correspond to low and high electricity prices, shown in green.

The value that the PTES systems add to the wind farm is highlighted by the increase in profit. Without the PTES system, for the same price and wind profile, this farm would generate £57,443.3 revenue. With the PTES system, the revenue increases to £59,144.3. This shifting ability also means that the wind power can be used for more dispatchable ancillary services such as frequency regulation and inertia control. These will add increased value to the system, or in other words, provide value stacking opportunities to the system. This study shows that the system under investigation here can be a viable alternative to established energy storage technologies and the SoC management algorithm is essential in the profitable and feasible operation of the system.

6. Conclusions

In this study, a steady-state model of a PTES system was built, and a rigorous initialization strategy was developed. The system was found to operate at 58.4 % efficiency at the design point, which is a competitive value within existing technologies. Particular attention was given to heat exchanger profiles, as this was identified as a research gap. Extensive internal heat exchange profiles were developed in Aspen

HYSYS. This was a vital study to conduct, considering the changes in the fluid properties with part-load conditions.

Additionally, a method was developed for estimating and managing state-of-charge. The state-of-charge of the system was differentiated into two distinct but interlinked categories: in-cycle and cycle-to-cycle SoC management. The capabilities of this method were demonstrated using several case studies of an average supply/demand scenario. Using in-cycle SoC management, the mismatch between the two storage tanks were reduced to, on average, 0.24 % in the case studies. Furthermore, these case studies, with different boundary conditions, demonstrated the effectiveness of cycle-to-cycle SoC management by ensuring optimal profitable operation in each scenario. Finally, the PTES system was simulated in a study where it was coupled with a wind farm. In the wind farm scenario, the average round-trip efficiency of the system fell to 46.5 % since the wind power capped the charging power and the system was forced to operate at off-design conditions more and more. This shows the necessity of operating at part-load conditions. It was shown that the addition of the PTES system allows for the wind farm to operate in a dispatchable manner and with increased profit. All of these results show the need to understand both the part-load behavior of the PTES system and SoC management methods. The system was, in part, limited by the maximum discharging power, which, with the given price profile, did not allow for extremely deep discharges throughout the simulation time horizon.

McTigue and Neises [30] analyzed a PTES system with a design very similar to the one presented in this paper, focusing on off-design operation. Their study examined the impact of varying the working fluid mass in circulation to control charging and discharging power. They investigated part-load operation down to 50 % of nominal design conditions for both charging and discharging, finding that roundtrip efficiency varied from 61 % to 57 %, with performance degrading at lower loads. In contrast, this study employs variable-speed turbomachinery to control charging and discharging power, reaching part-load operation down to 55 % for charging and 25 % for discharging. This approach yields a wider range of roundtrip efficiencies, from 60 % to 33 %, with an average roundtrip efficiency of 42 % for the wind farm integration case. While direct comparison is challenging due to the differing control methods, the observed part-load performance values are generally comparable. A dynamic model is necessary to directly compare the advantages and disadvantages of each part-load operation strategy. We intend to use the findings of this paper as a foundation for future dynamic modelling and control studies.

For further research, there is potential of implementing heat integration applications to the PTES system, which will also require SoC management between the tanks. As the storages are used to provide heating or cooling, the SoC estimation needs to be updated to maintain feasible operation. SoC management as a means of augmenting existing control strategies can be proposed. With the addition of cycle-to-cycle SoC management, any current control strategies would be better suited to handle changes in energy supply and demand.

Future studies in this field should:

- 1) Implement heat integration to the system where the hot side can provide high grade heat to a coupled industrial process.
- 2) Investigate the limiting effects of maximum charge and price curve shape. Also, it may prove useful to investigate the tank size effects but less so the aforementioned variables.
- 3) Include turbine maps in addition to compressors and use more optimal turbomachinery data. If this is done, the sparseness issue of the load levels can be resolved.
- 4) Build a comprehensive dynamic model to implement the SoC management methods, in addition to control strategies to ascertain the methods' capabilities in real-time operation scenarios.
- 5) A more in-depth analysis of integration studies with renewable sources is required, considering sizing of the both the storage system and the integrated power supply.

CRedit authorship contribution statement

Alp Albay: Writing – review & editing, Writing – original draft, Visualization, Methodology, Formal analysis, Conceptualization. **Zhennan Zhu:** Writing – review & editing, Writing – original draft, Supervision, Methodology. **Mehmet Mercangöz:** Writing – review & editing, Supervision, Methodology, Funding acquisition, Conceptualization.

Declaration of competing interest

The authors declare the following financial interests/personal relationships which may be considered as potential competing interests: Mehmet Mercangoz reports financial support was provided by Engineering and Physical Sciences Research Council. Zhennan Zhu reports financial support was provided by Engineering and Physical Sciences Research Council. If there are other authors, they declare that they have no known competing financial interests or personal relationships that could have appeared to influence the work reported in this paper.

Appendix A

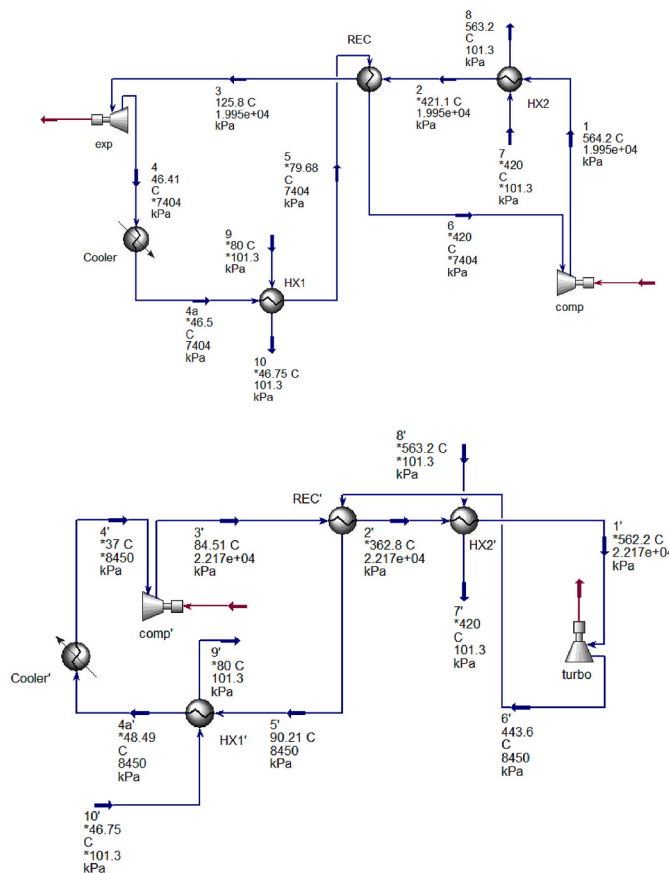


Fig. A1. Aspen flowsheets for a) charge cycle, b) discharge cycle [33].

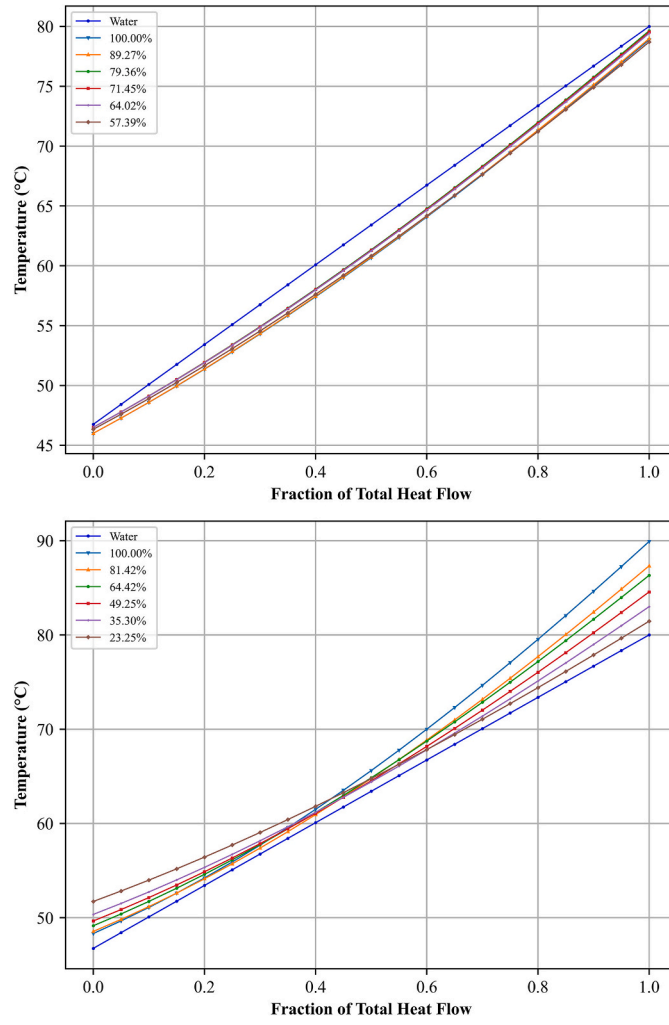


Fig. A2. Cold side heat exchanger temperature profiles at all loads.

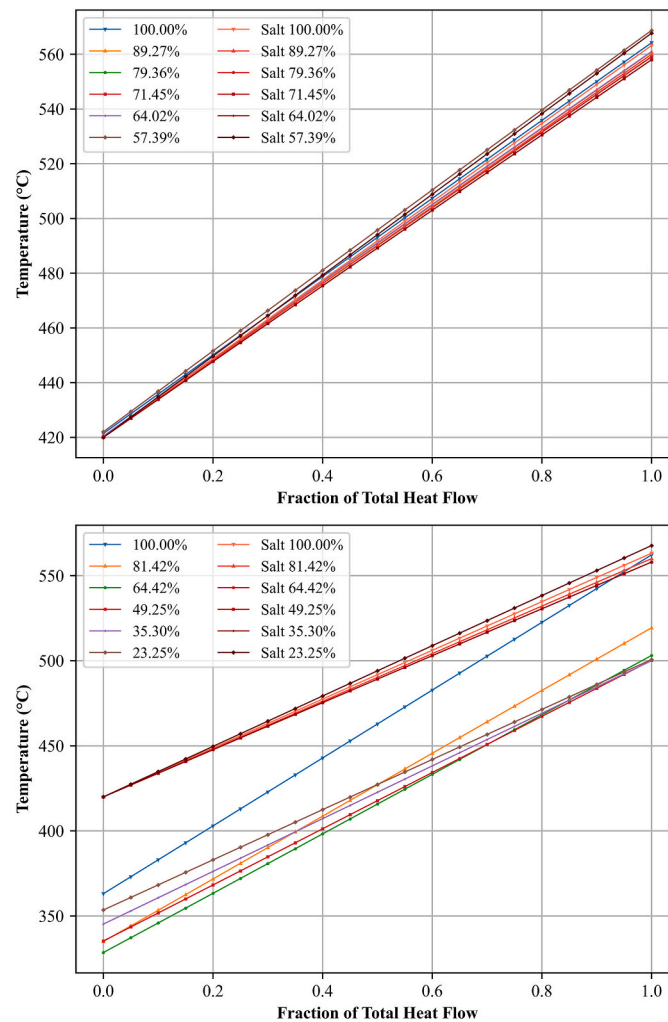


Fig. A3. Hot side heat exchanger temperature profiles at all loads.

Data availability

Data will be made available on request.

References

- [1] H. Ritchie, P. Rosado, M. Roser, Energy production and consumption, URL, <https://ourworldindata.org/energy-production-consumption>, 2023.
- [2] T. Jia, P. Dou, P. Chu, Y. Dai, Proposal and performance analysis of a novel solar-assisted resorption-subcooled compression hybrid heat pump system for space heating in cold climate condition, *Renew. Energy* 150 (2020) 1136–1150, <https://doi.org/10.1016/j.renene.2019.10.062>.
- [3] T. Jia, P. Chu, P. Dou, Y. Dai, Working domains of a novel solar-assisted gas-based two-stage absorption-resorption heat pump with multiple internal heat recovery for space heating, *Energy Convers. Manag.* 220 (2020) 113060, <https://doi.org/10.1016/j.enconman.2020.113060>.
- [4] M. Arita, A. Yokoyama, Y. Tada, Evaluation of battery system for frequency control in interconnected power system with a large penetration of wind power generation, *IEEE* (2006) 1–7, <https://doi.org/10.1109/icpst.2006.321682>.
- [5] J.A. Dowling, K.Z. Rinaldi, T.H. Ruggles, S.J. Davis, M. Yuan, F. Tong, N.S. Lewis, K. Caldeira, Role of long-duration energy storage in variable renewable electricity systems, *Joule* 4 (2020) 1907–1928, <https://doi.org/10.1016/j.joule.2020.07.007>.
- [6] M.C. Argyrou, P. Christodoulides, S.A. Kalogirou, Energy storage for electricity generation and related processes: technologies appraisal and grid scale applications, *Renew. Sust. Energy Rev.* 94 (2018) 804–821, <https://doi.org/10.1016/j.rser.2018.06.044>. URL, <https://www.sciencedirect.com/science/article/pii/S0306261914010290>.
- [7] A. Gil, M. Medrano, I. Martorell, A. Lázaro, P. Dolado, B. Zalba, L.F. Cabeza, State of the art on high temperature thermal energy storage for power generation. part 1—concepts, materials and modellization, *Renew. Sust. Energy Rev.* 14 (2010) 31–55, <https://doi.org/10.1016/j.rser.2009.07.035>. URL, <https://www.sciencedirect.com/science/article/pii/S1364032109001774>.
- [8] D. Miron, A. Navon, Y. Levron, J. Belikov, C. Rotschild, The costcompetitiveness of concentrated solar power with thermal energy storage in power systems with high solar penetration levels, *Journal of Energy Storage* 72 (2023) 108464, <https://doi.org/10.1016/j.est.2023.108464>.
- [9] T. Desrues, J. Ruer, P. Marty, J. Fourmigué, A thermal energy storage process for large scale electric applications, *Appl. Therm. Eng.* 30 (2010) 425–432, <https://doi.org/10.1016/j.applthermaleng.2009.10.002>.
- [10] SwRI, 2022 annual summary, URL, <https://www.swri.org/newsroom/annual-report/2022>, 2022.
- [11] J.M. Henry, F. Maurer, J.-L. Drommi, T. Sautereau, Converting to variable speed at a pumped-storage plant (09 2013), URL, <https://www.renewableenergyworld.com/storage/converting-to-variable-speed>.
- [12] B. Xingyan, X. Wang, R. Wang, J. Cai, H. Tian, G. Shu, Optimal selection of supercritical CO₂ brayton cycle layouts based on part-load performance, *Energy* 256 (2022) 124691, <https://doi.org/10.1016/j.energy.2022.124691>.
- [13] M.T. White, G. Bianchi, L. Chai, S.A. Tassou, A.I. Sayma, Review of supercritical CO₂ technologies and systems for power generation, *Appl. Therm. Eng.* 185 (Feb. 2021) 116447, <https://doi.org/10.1016/j.applthermaleng.2020.116447>.
- [14] A. Benato, A. Stoppato, Pumped thermal electricity storage: a technology overview, *Thermal Science and Engineering Progress* 6 (2018) 301–315, <https://doi.org/10.1016/j.tsep.2018.01.017>.
- [15] AIP Conference Proceedings, Supercritical CO₂ heat pumps and power cycles for concentrating solar power. doi:<https://doi.org/10.1063/5.0090002>.
- [16] P. Wu, Y. Ma, C. Gao, W. Liu, J. Shan, Y.-P. Huang, J. Wang, D. Zhang, X. Ran, A review of research and development of supercritical carbon dioxide brayton cycle technology in nuclear engineering applications, *Nucl. Eng. Des.* 368 (2020) >110767, <https://doi.org/10.1016/j.nucengdes.2020.110767>.
- [17] G. Angelino, Carbon dioxide condensation cycles for power production, *Journal of Engineering for, Power* 90 (1968) 287–295, <https://doi.org/10.1115/1.3609190>.

- [18] Y. Liu, Y. Wang, D. Huang, Supercritical CO₂ Brayton cycle: a state-of-the-art review, *Energy* 189 (2019) 115900, <https://doi.org/10.1016/j.energy.2019.115900>.
- [19] T. Neises, C. Turchi, A comparison of supercritical carbon dioxide power cycle configurations with an emphasis on CSP applications, *Energy Procedia* 49 (2014) 1187–1196, <https://doi.org/10.1016/j.egypro.2014.03.128>.
- [20] M. Marchionni, G. Bianchi, S.A. Tassou, Review of supercritical carbon dioxide (SCO₂) technologies for high-grade waste heat to power conversion, *SN, Appl. Sci.* 2 (03 2020), <https://doi.org/10.1007/s42452-020-2116-6>.
- [21] M. Morandin, F. Maréchal, M. Mercangöz, F. Buchter, Conceptual design of a thermo-electrical energy storage system based on heat integration of thermodynamic cycles – part A: methodology and base case, *Energy* 45 (2012) 375–385, <https://doi.org/10.1016/j.energy.2012.03.031>.
- [22] Z. Ma, J. Gifford, X. Wang, J. Martinek, Electric-thermal energy storage using solid particles as storage media, *Joule* 7 (2023) 843–848, <https://doi.org/10.1016/j.joule.2023.03.016>.
- [23] J.-M. Yin, Q.-Y. Zheng, Z.-R. Peng, X.-R. Zhang, Review of supercritical CO₂ power cycles integrated with CSP, *Int. J. Energy Res.* 44 (2019) 1337–1369, <https://doi.org/10.1002/er.4909>.
- [24] B.D. Iverson, T.M. Conboy, J.J. Pasch, A.M. Kruiuzenga, Supercritical CO₂ Brayton cycles for solar-thermal energy, *Appl. Energy* 111 (2013) 957–970, <https://doi.org/10.1016/j.apenergy.2013.06.020>. <https://www.sciencedirect.com/science/article/pii/S0306261913005278>.
- [25] J. McTigue, P. Farres-Antunez, K. Elingwood, T. Neises, A. White, Pumped thermal electricity storage with supercritical CO₂ cycles and solar heat input, in: The VII International Young Researchers' Conference – Physics, Technology, Innovations (PTI-2020), 2020, <https://doi.org/10.1063/5.0032337>.
- [26] G.F. Frate, L. Paternostro, L. Ferrari, U. Desideri, Off-design of a pumped thermal energy storage based on closed Brayton cycles, *J. Eng. Gas Turbines Power* (09 2021), <https://doi.org/10.1115/1.4052426>.
- [27] J. Yang, Z. Yang, Y. Duan, Part-load performance analysis and comparison of supercritical CO₂ Brayton cycles, *Energy Convers. Manag.* 214 (2020) 112832, <https://doi.org/10.1016/j.enconman.2020.112832>.
- [28] T. J. Held, J. Miller, J. Mallinak, V. Avadhanula, and L. Magyar, "Pilot-scale testing of a transcritical CO₂-based pumped thermal energy storage (PTES) system," Volume 6: Education; Electric Power; Energy Storage; Fans and Blowers, Jun. 2024, doi:<https://doi.org/10.1115/gt2024-129211>.
- [29] N.R. Smith, J. Just, J. Johnson, F. Karg-Bulnes, Performance Characterization of a Small-scale Pumped Thermal Energy Storage System, Jun. 2023, <https://doi.org/10.1115/gt2023-104232>.
- [30] J. McTigue, T. Neises, Off-design operation and performance of pumped thermal energy storage, *Journal of Energy Storage* 99 (Oct. 2024) 113355, <https://doi.org/10.1016/j.est.2024.113355>.
- [31] M. Pettinari, G.F. Frate, K. Kyprianidis, L. Ferrari, Dynamic modelling and part-load behavior of a Brayton heat pump, in: Linköping Electronic Conference Proceedings, 2023, <https://doi.org/10.3384/ecp200033>.
- [32] A. Ghilardi, G.F. Frate, K. Kyprianidis, M. Tucci, L. Ferrari, Brayton pumped thermal energy storage: optimal dispatchment in multi-energy districts, *Energy Convers. Manag.* 314 (Aug. 2024) 118650, <https://doi.org/10.1016/j.enconman.2024.118650>.
- [33] AspenTech, AspenHYSYS V12.2, Available: Aspen Tech, Nov. 2021. <https://www.aspentech.com/en/products/engineering/aspen-hysys>.
- [34] D. Kearney, U. Herrmann, P. Nava, B. Kelly, R. Mahoney, J. Pacheco, R. Cable, N. Potrovitza, D. Blake, H. Price, Assessment of a molten salt heat transfer fluid in a parabolic trough solar field, *Journal of Solar Energy Engineering* 125 (2003) 170–176, <https://doi.org/10.1115/1.1565087>. URL, <https://www.nrel.gov/docs/fy03osti/40028.pdf>.
- [35] J.D. McTigue, P. Farres-Antunez, C.N. Markides, A. White, Pumped thermal energy storage with liquid storage, in: Elsevier eBooks, 01 2021, <https://doi.org/10.1016/b978-0-12-819723-3.00054-8>.
- [36] P. Jiang, B. Wang, Y. Tian, X. Xu, L. Zhao, Design of a supercritical CO₂ compressor for use in a 1 MWe power cycle, *ACS Omega* 6 (2021) 33769–33778, <https://doi.org/10.1021/acsomega.1c05023>.
- [37] J. J. Pasch, T. M. Conboy, D. Fleming, G. E. Rochau, Supercritical CO₂ Recompression Brayton Cycle: Completed Assembly Description. (10 2012). doi:<https://doi.org/10.2172/1057248>.
- [38] N. Tsuzuki, Y. Kato, T. Ishiduka, High performance printed circuit heat exchanger, *Appl. Therm. Eng.* 27 (2007) 1702–1707, <https://doi.org/10.1016/j.applthermaleng.2006.07.007>.
- [39] E. W. Lemmon, I. H. Bell, M. L. Huber, M. O. McLinden, NIST Standard Reference Database 23: Reference Fluid Thermodynamic and Transport Properties-REFPROP, Version 10.0, National Institute of Standards and Technology (2018).
- [40] E. Tsoutsanis, Y.G. Li, P. Pilidis, M. Newby, Part-load performance of gas turbines: part I — a novel compressor map generation approach suitable for adaptive simulation, in: ASME 2012 Gas Turbine India Conference, 12 2012, <https://doi.org/10.1115/gtindia2012-9580>.
- [41] Nord Pool, N2EX day ahead auction prices, Nordpoolgroup.com, Dec. 17, 2024. <https://data.nordpoolgroup.com/>. (Accessed 17 December 2024).
- [42] S. Bolusani, et al., The SCIP Optimization Suite 9.0, arXiv.org, 2024. <https://arxiv.org/abs/2402.17702>. (Accessed 14 August 2024).
- [43] A. Wächter, L.T. Biegler, On the implementation of an interior-point filter line-search algorithm for large-scale nonlinear programming, *Mathematical Programming* 106 (1) (Apr. 2005) 25–57, <https://doi.org/10.1007/s10107-004-0559-y>.
- [44] Great Britain National Grid status, Available: gridwatch.emplar.co.uk, 2016. <https://www.gridwatch.emplar.co.uk>.